DOI: 10.21120/LE/19/1/3

Acta Geographica Debrecina
Landscape & Environment series 19 (1) 2025. 29-40

SATELLITE DERIVED BATHYMETRY (SBD) OF INACCESSIBLE WATER: AN APPLICATION OF LOG-TRANSFORMED BAND RATIO MODEL

KAMAL NAG

[1]Prabhat Kumar College, Department of Geography, Contai, West Bengal, India
Email: kamal.nag@gmail.com

Received 5 May 2024, accepted in revised form 30 May 2024

Abstract
The present study applied log transformed Band Ratio Model (BRM) on Sentinel-2A image of Copernicus programme of European Space Agency (ESA) to derive shallow water bathymetric map in a part of Indian eastern coast. The "empirical bathymetry processor" in SNAP software of ESA has been used for this purpose. General Bathymetric Chart of the Ocean (GEBCO)_2020 of Nippon Foundation has been taken as a reference image for point data input. Log transformed ratio of band-2 and ban-3 of Sentinel-2A at 10 m spatial resolution enables bathymetric mapping of nearshore water. Before applying BRM, image processing involves land mask, sun glint correction and dark object subtraction (DOS). This approach can be used as an alternative to conventional hydrographic survey for bathymetric mapping in inaccessible water with great savings of cost and time.

Keywords: Sentinel-2A, Band Ratio Model (BRM), SNAP software, GEBCO_2020, bathymetric mapping, inaccessible water

1. Introduction

Satellite-Derived Bathymetry (SDB) brings new opportunities to the marine research community. Surveying shallow waters now requires minimum mobilisation of persons and equipment. Hydrographic surveying methods involving ship-based acoustic systems need high-cost resources. In comparison to hydrographic surveying, space technology based SDB provides rapid access to shallow water bathymetric data and saves costs (Chénier et al. 2018). SDB is obtained by transforming the surface reflectance of shallow waters to the depth of the water column. During recent years, a number of SDB models have evolved (Gao 2009; Gholamalifard et al. 2013; Geyman 2019). "Empirical bathymetry" is one of such model. Efficiency of this model to generate shallow water bathymetric charts has been tested in a few research works so far (Flener et al. 2010; Gholamalifard et al. 2013; Hamylton et al. 2015). Different studies have proved that Sentinel 2A data product is a potent medium of deriving nearshore bathymetry (Hedley et al. 2018; Bolaños et al. 2018; Caballero et al. 2000; Mateo-Pérez et al. 2020). Geomorphological change in nearshore zone is a continuous event and it require constant vigilance for a hassle-free maritime trade, to monitor nearshore marine

habitat and to protect coastal community from marine hazards. Rapid development of sensor's capacity to capture data at minute level from the space, makes it possible to derive bathymetry at regular interval and apply the result day to day need of coastal management. SDB is of extremely useful to identify nearshore isobaths and its changes over time and detection of such changes facilitate port authority for smooth function of port activities (Pacheco et al. 2015). Depth of nearshore zone is an important determinant to quantify the spatial extent of coastal flood (Kirwan et al. 2012). Prediction of coastal flood with higher degree of accuracy depends on accuracy of nearshore bathymetry and frequency of availing such bathymetric chart as the depth of nearshore zone is no constant parameter (Hay et al. 1993). Ecosystem productivity of nearshore zone is also depth dependant as the reach of sunlight is limited only in photic zone. Spatial extent of coastal benthic vegetation and their productivity changes with the change in nearshore depth (Gattuso et al. 2006). Frequent observation of nearshore bathymetry become essential to predict habitat changes and its management.

Present study aims to derive bathymetry by applying this model on Sentinel 2A multispectral image. Depth of reference points was derived from General Bathymetric Chart of the Ocean (GEBCO) 2020 and such point data of depth has been used as an alternative to in-situ point data which is usually collected through an echo-sounder. This alternative method may holds significance especially for inaccessible water where either hydrographic survey of in-situ data collection for SDB is difficult.

2. Study Area

The study has been conducted along a part of eastern coast of India. The coastal tract is located in the Indian state of Odisha. It is extended towards the south for a distance of about 7 km, starting from the entry point of Paradip port (20° 14' 8.12"N and 86° 36' 54.22"E to 20° 15' 29.95"N and 86° 40' 34.46"E). Commonly this part of the Odisha coast is known as Paradip coast (Fig. 1).

Table 1. Spatial Resolution of Sentinel 2A MSI

Band Number	Central Wavelength (nm)	Bandwidth (nm)	Spatial Resolution (m)
1	443	20	60
2	490	65	10
3	560	35	10
4	665	30	10
5	705	15	20
6	740	15	20
7	783	20	20
8	842	115	10
8a	865	20	20
9	945	20	60
10	1375	30	60
11	1610	90	20
12	2190	180	20
TCI*	RGB	Composite	10

Source: https://scihub.copernicus.eu

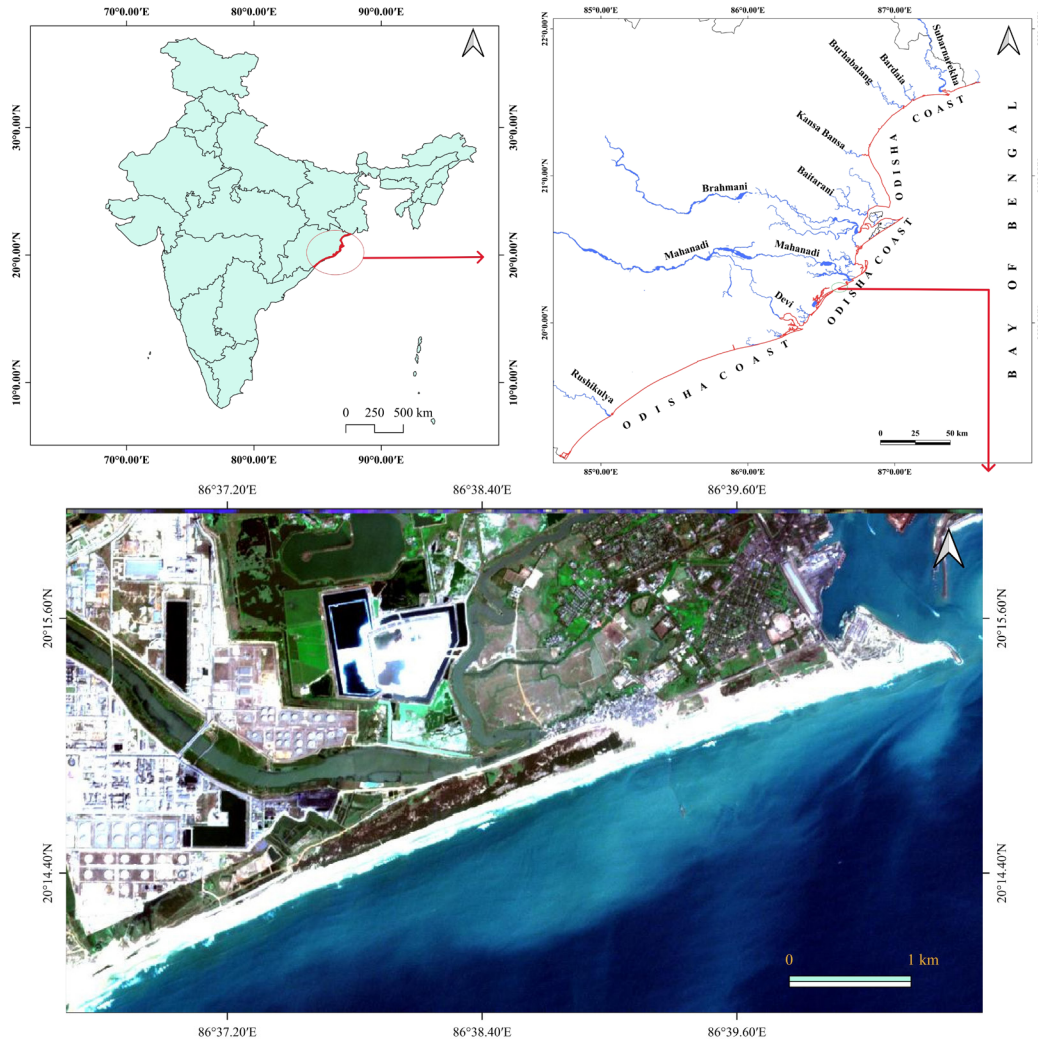

Fig. 1. (c) RGB view of Sentinel 2A image, Paradip coast

3. Materials and Methods

Sentinel-2A Multispectral Images (MSI) have been used to determine nearshore bathymetry. The European Space Agency's (ESA) Multispectral Instrument on the Sentinel-2A satellite acquires 13 spectral bands ranging from Visible and Near-Infrared (VNIR) to Shortwave Infrared (SWIR) wavelengths along a 290-km orbital swath. Blue (490 nm), green (560 nm), red (665 nm), and near-infrared (842 nm) bands acquire data at 10 metre spatial resolution. Spectral and spatial resolution of all 13 bands have been outlined in Table 1. Level-2A data products which have been used in this study include a scenes classification and an atmospheric correction applied to Top-Of-Atmosphere (TOA) Level-1C ortho-image products. Level-2A main output is an ortho-image Bottom-Of-Atmosphere (BOA) corrected reflectance product (User Guide, Sentinel-2A, https://sentinel.esa.int/). Specifications of image scene used in this study have been outlined in Table 2.

SDB was developed in the Sentinel Application (SNAP 8.0.0) software developed

Table 2. Specifications of Sentinel 2A MSI

Sensing Date	05-03-2021
Filename	S2A_MSIL2A_20210305T043701_N0214_R033_ T45QVC_20210305T073436.SAFE
Identifier	S2A_MSIL2A_20210305T043701_N0214_R033_ T45QVC_20210305T073436
Instrument	Multi-Spectral Instrument
Satellite	Sentinel-2
Processing level	Level-2A
Cloud cover percentage	0.053486
Dark features percentage	0.911468
Granule identifier	S2A_OPER_MSI_L2A_TL_VGS1_20210305T073436_A029774_T45QVC_ N02.14
Illumination Azimuth Angle	136.8521383
Illumination Zenith Angle	34.6838800225588
Source: https://scihub. copernicus.eu	

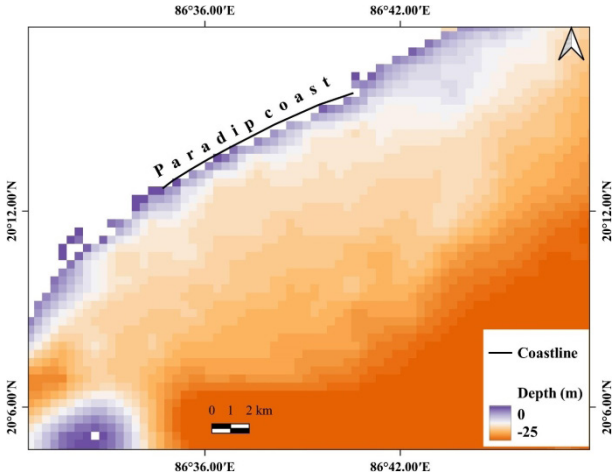

Fig. 2. General Bathymetric Chart of the Oceans (GEBCO)_2020, Paradip coast

by ESA. "Empirical Bathymetry Processor" tool in the "Sen2Coral" processor has been installed and used in SNAP to derive shallow water bathymetry. General Bathymetric Chart of the Oceans (GEBCO) _2020 (GEBCO has been developed through the Nippon Foundation-GEBCO Seabed 2030 Project. GEBCO_2020 Grid provides global coverage of elevation and bathymetry data on a 400 ×400 m grid) has been used to generate a bathymetry point data file which is an essential prerequisite to run this processor (Fig. 2).

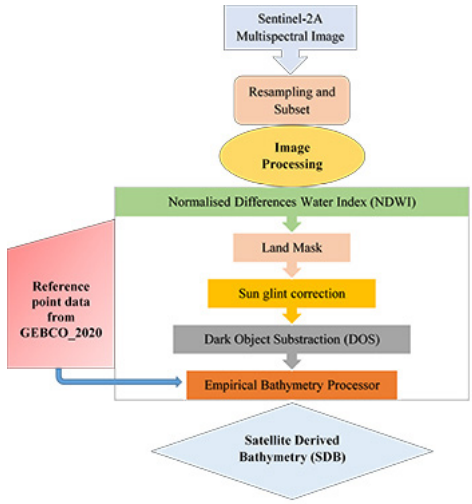

Fig. 3. Workflow for SDB

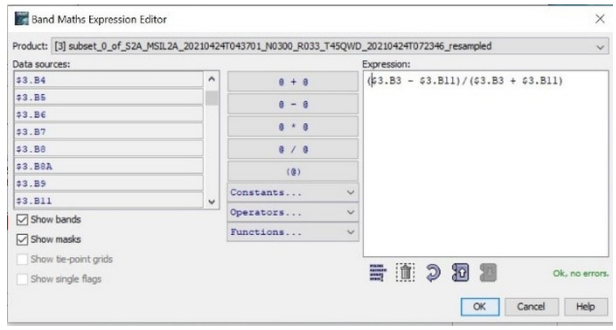

Fig. 4. Expression for NDWI in Band Maths expression editor of SNAP 8.0.0

At the pre-processing stage entire set of thirteen bands of Sentinel-2A product has been resampled into the pixel resolution of band-2 (i.e. 10 m) and Region of interest (ROI) cut out though "subset" tool in SNAP. the following steps of image processing includes Normalised Differences Water Index (NDWI), Land Mask, sun glint correction Dark Object Subtractions (DOS) and employing empirical bathymetry model (Fig. 3). NDWI algorithm has been applied to MSI in SNAP through "Band math" tool. NDWI may be defined as equation (1) (McFeeters 1996; Gao 1996; Xu 2006)

$$NDWI = \frac{Green - NIR}{Green + NIR} \quad (1)$$

The algorithm was written in "Band math" through "expression" box as equation (2) (Fig 4).

$$NDWI = \frac{Band\ 3 - Band\ 11}{Band\ 3 + Band\ 11} \quad (2)$$

"Land Mask" function was run to transform all pixels on land with no-data-value. "Land/ Sea Mask" tool in SNAP was used to run this operation. Processing parameters were set up by selecting all 13 primary bands as source bands and a new vector was created based

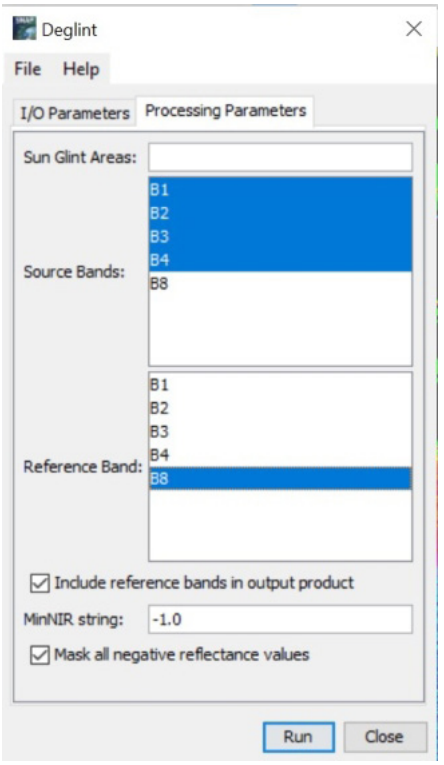

Fig. 5. Deglint processing module in SNAP 8.0.0 software

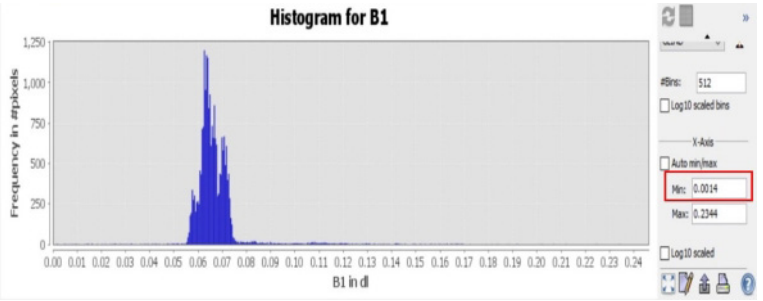

Fig. 6. Histogram for band-1 with information on minimum and maximum pixel values

on NDWI to use it as a mask. This function produces a new band set with a land/sea mask band which was used in subsequent stages. Glint correction was performed to remove contribution of the direct reflectance from the top of the atmosphere (TOA) water interface from the imagery. Present study adopted the glint correction algorithm as formulated by Hedley et al. (Hedley et al. 2005). If sun glint correction was to be applied on Band-i, then the equation may be written as equation (3).

$$R_i' = R_i - b_i(R_{NIR} - Min_{NIR}) \qquad (3)$$

Where

R_i' = Sun-glint corrected pixel

R_i = Pixel which was to be deglinted

b_i = Regression slope of bivariate regression

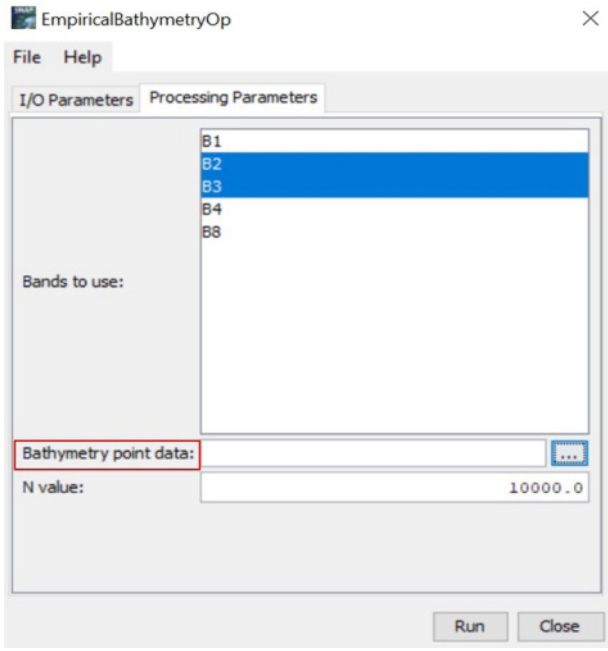

Fig. 7. Empirical Bathymetry Processing module in SNAP 8.0.0 software

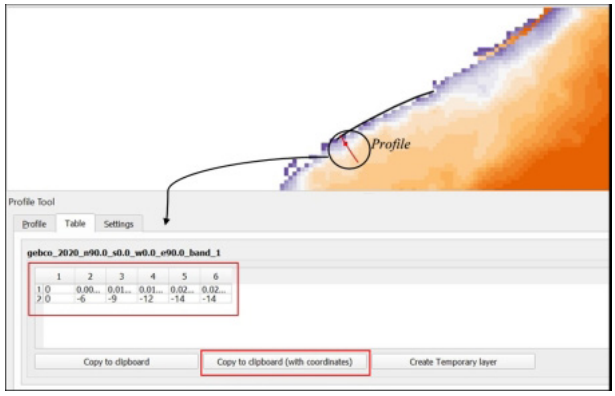

Fig. 8. Profile tool in QGIS 3.14 "Pi"

of pixel value Band-i and NIR Band.

(R_{NIR}-Min_{NIR}) = Difference between the pixel NIR value (R_{NIR}) and the ambient NIR level (Min_{NIR})

Glint corrected image has been developed in SNAP with the "Deglint '' processing module of "Sen2Coral processor" tool (Fig. 5). Dark Object Subtraction (DOS) was the next atmospheric correction followed by deglint. It aims at removing shadow areas from the image (De Keukelaere 2018). Minimum reflectance value was subtracted from the image through the "band math" tool. This minimum value was obtained from the histogram of the respective band (Fig. 6).

After DOS, the final task towards generating SDB was applying the "Empirical Bathymetry Processor" tool. This processor derives bathymetry through a log-transformed band ratio model (BRM). This model uses

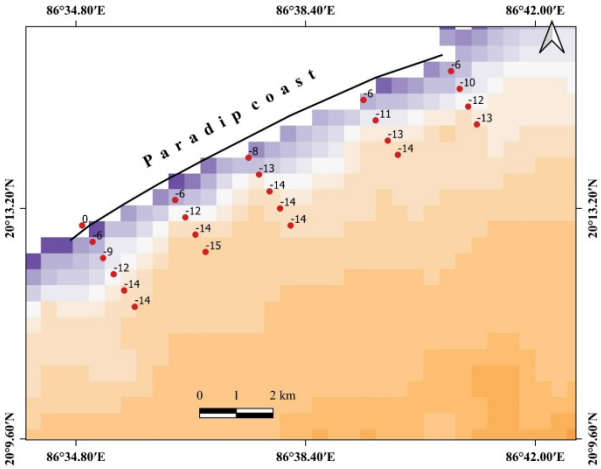

Fig. 9. Reference points location and depths (m), derived from GEBCO_2020

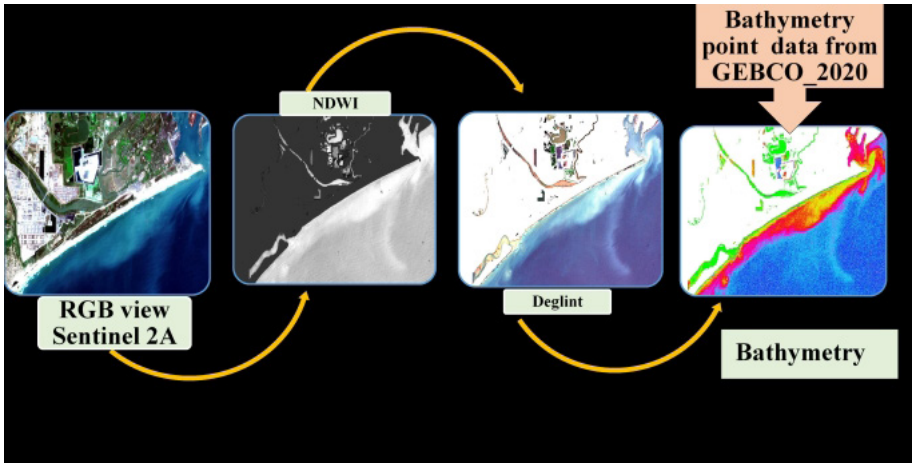

Fig. 10. Stages of bathymetry band generation from Sentinel 2A MSI

a ratio of water reflectance of bands having different water absorptions. According to Stumpf and Holderied (Stumpf 2003), the ratio of reflectance will change with depth. The log-transform of bands accounts for the exponential decrease of light with depth. Blue light (440–500 nm) has a penetrating capacity of 25 m depth at least. Green light get absorbed faster than blue with increasing depth. A ratio of these two bands provides bathymetric information in nearshore up to 25 m depth. They have defined SDB as equation (4).

$$SDB = M_1 pSDB - M_0 \quad (4)$$

Where

pSDB= Relative depth from Satellite

M_1 and M_0= The constants m1 and m0 are estimated by linear regression over the in-situ sample points.

and

$$\text{pSDB} = \frac{ln(n\,\pi\,R_{rs}(\lambda_i))}{ln(n\,\pi\,R_{rs}(\lambda_j))} \quad (5)$$

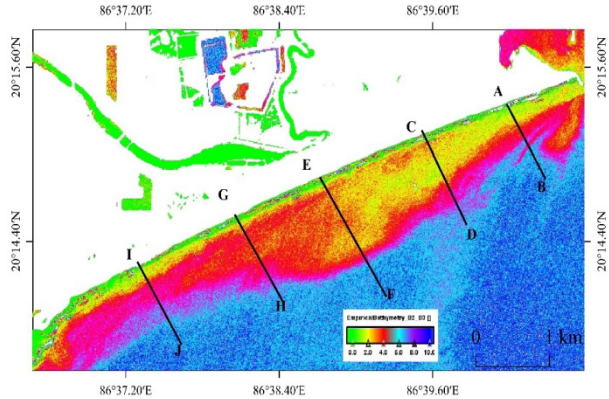

Fig. 11. Cross-shore profiles on Sentinel-2A derived bathymetric map

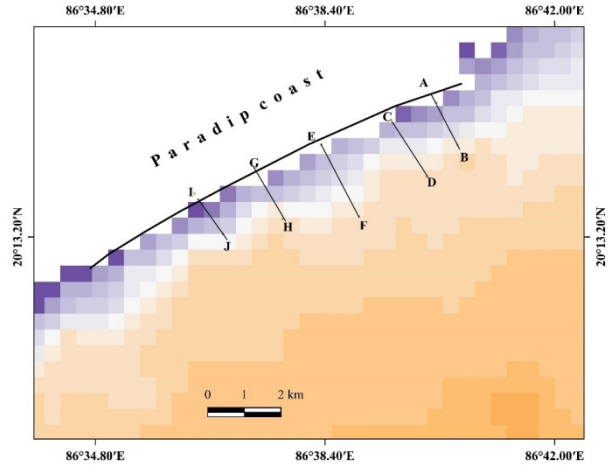

Fig. 12. Cross-shore profile on GEBCO_2020

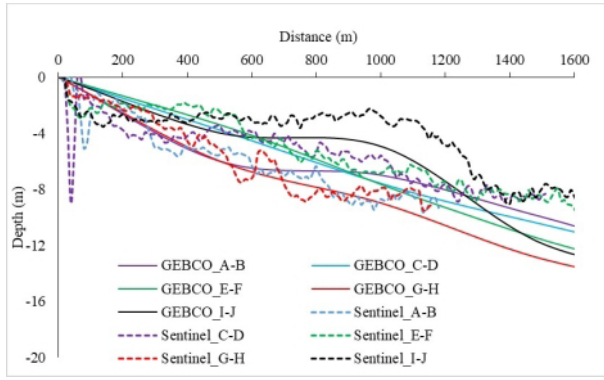

Fig. 13. Superimposed profiles drawn across GEBCO_2020 and Sentinel-2A

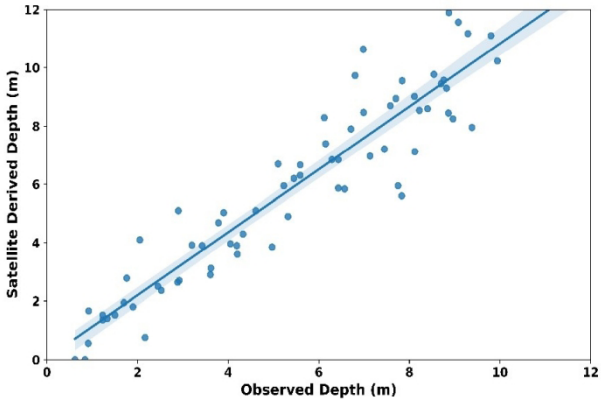

Fig. 14. Regression plot of observed depth Vs. Satellite derived depth

$R_{rs}(\lambda_i)$ and $R_{rs}(\lambda_j)$ are two different sunglint corrected bands. In this study sunglint corrected Band 3 and Band 2 were used as λ_i and λ_j respectively.

N = 1000 is a fixed constant for all areas

(Caballero et al. 2019)

"Empirical Bathymetry Processor" requires bathymetry point data to use as a reference (Fig. 7). For that purpose, a text file was created with comma separated information on latitude, longitude and depth. Point data of depth has been derived through "profile" tool in QGIS 3.14 "Pi" (Fig. 8). Reference point bathymetry data of GEBCO_2020 were copied and paste in MS Excel sheet and save as comma separated ".txt" file. Reference points depths derived from GEBCO_2020 have been mapped in QGIS (Fig.9) for cross verification with Sentinel 2A derived bathymetry. A new "bathymetry band" was developed through this "Empirical Bathymetry Processor" tool (Fig. 10). Bathymetric profile was drawn from this band by using the "profile" tool in SNAP and exporting data to MS excel. For the purpose of map composition, this single band image was exported as a "GeoTiff" file and opened in QGIS 3.14 "Pi" platform.

4. Results and Discussion

The SDB of Paradip coast reveals how depth changes in the nearshore zone. Five cross-shore Profiles have been drawn across the nearshore zone (Fig. 11). Profiles A-B, C-D, E-F, G-H and I-J run for a distance of 1160 m, 1630 m, 2090 m, 1510 m and 1180 m respectively. The length of a profile was obtained by multiplying spatial resolution of pixels (i.e., 10 m) with the number of pixels through which the profile ran. Maximum depth (9.82 m) has been observed along the C-D profile at a distance of 1610 m (equivalent to 161 pixel distance) from shoreline. Five profiles with the same geographical extension have been drawn on GEBCO_2020 (Fig. 12) and superimposed on Sentinel 2A derived profiles (Fig. 13). Superimposed graphical plot indicates Sentinel 2A derived profiles are more capable of providing more detailed minutes than GEBCO_2020 derived profiles. The 15 arc second grid of GEBCO_2020 is too small to capture bathymetric irregularities over a short distance. However, it is indicative of pattern of depth changes. An important observation on superimposed profiles plot also indicates that as the distance and depth increases from shoreline these two sets of profile tend to deviate. After a distance of 1400 m from shoreline, average depth of Sentinel 2A derived profiles is less than the depth of GEBCO_2020 profiles.

To find out the accuracy of satellite-based depth measurements against traditional, observed measurements, a set of seventy unused data point collected through field based measurement and a regression analysis was performed. The regression

plot of Observed Depth vs Satellite Derived Depth with a 95% confidence interval, provides several insights. The plot shows a strong linear relationship between the observed and satellite-derived depths. This is consistent with the high R-squared value of 0.983, indicating that the satellite-derived measurements explain approximately 98.3% of the variance in the observed measurements. The shaded area around the regression line represents the 95% confidence interval (Fig. 14). This interval is relatively narrow, suggesting that the predictions made by the regression model are quite precise. The Mean Squared Error (MSE) and Root Mean Squared Error (RMSE) values are 14.53 and 3.81, respectively. These values indicate the average squared difference and the average absolute difference between the observed and predicted values. Given the high R-squared value, these error metrics are relatively low, further supporting the accuracy of the satellite-derived measurements. Overall, the analysis suggests that satellite-based depth measurements are highly accurate and reliable when compared to traditional observed measurements, especially in shallow sea within a depth of 10m.

5. Conclusions

This study indicates the applicability of Sentinel-2A imagery to successfully derived bathymetry at 10 m spatial resolution. Bathymetric charts of inaccessible water can be successfully created from Sentinel-2A with log transformed band ratio model (BRM). Reference point input from GEBCO_2020 may be used as an alternative to in-situ point data collection through Echo sounder. The image processing and application of "empirical bathymetry processor" in SNAP software hold immense potential to reveal bathymetry of inaccessible water. Present approach of uncovering bottom topography of nearshore water is time and cost-saving. Such a bathymetric map can be applied for many purposes such as identifying location of port and harbours, coastal vulnerability indexing, bathymetric change detection etc.

The future of satellite-derived bathymetry promises a paradigm shift in our understanding and utilization of nearshore bathymetry. With advancements in remote sensing technologies and data processing algorithms, satellite-derived bathymetry is poised to become more accurate, accessible, and comprehensive. Although, the results of this study and level of accuracy are very encouraging, future endeavour must direct to inquire SDB in deep water, beyond 15m. High-resolution satellite imagery coupled with machine learning algorithms enables the derivation of bathymetric data with higher degree of precision, in shallow and turbid waters where traditional methods face limitations. This burgeoning field holds immense potential for various applications, including marine navigation, resource exploration, environmental monitoring, and coastal zone management. As satellite constellations expand and sensor technologies evolve, the future of satellite-derived bathymetry holds the promise of unlocking new insights into the Earth's submerged landscapes and fostering sustainable use and conservation of our marine environments.

6. References

Chénier, R. - Faucher, M. A. - Ahola, R. (2018). Satellite-Derived Bathymetry for Improving Canadian Hydrographic Service Charts. ISPRS International Journal of GeoInformation, 7(8), 306. doi:10.3390/ijgi7080306

Gao, J. (2009). Bathymetric mapping by means of remote sensing: methods, accuracy and limitations. Progress in Physical Geography, 33(1),103–116. doi:10.1177/0309133309105657

Gholamalifard, M. - Esmaili-Sari, A. - Abkar, A. - Naimi, B. (2013). Bathymetric Modeling from Satellite Imagery via Single Band Algorithm (SBA) and Principal Components Analysis (PCA) in Southern Caspian Sea. Int. J. Environ. Res, 7(4), 877-886

Geyman, E. C. - Maloof, A. C. (2019). A Simple Method for Extracting Water Depth From Multispectral Satellite Imagery in Regions of Variable Bottom

Type. Earth and Space Science, 6(3), 527–537. doi:10.1029/2018ea000539

Flener, C. - Lotsari, E. - Alho, P. - Käyhkö, J. (2010). Comparison of empirical and theoretical remote sensing based bathymetry models in river environments. River Research and Applications, 28(1), 118–133. doi:10.1002/rra.1441

Gholamalifard, M. - Kutser, T. - Esmaili-Sari, A. - Abkar, A. A. - Naimi, B. (2013). Remotely Sensed Empirical Modeling of Bathymetry in the Southeastern Caspian Sea. Remote Sensing, 5(6), 2746-2762. https://doi.org/10.3390/rs5062746

Hamylton, S. M. - Hedley, J. D. - Beaman, R. J. (2015). Derivation of High-Resolution Bathymetry from Multispectral Satellite Imagery: A Comparison of Empirical and Optimisation Methods through Geographical Error Analysis. Remote Sensing, 7(12), 16257-16273. https://doi.org/10.3390/rs71215829

Hedley, J. D. - Roelfsema, C. - Brando, V. - Giardino, C. - Kutser, T. - Phinn, S. - Koetz, B. (2018). Coral reef applications of Sentinel2: Coverage, characteristics, bathymetry and benthic mapping with comparison to Landsat 8. Remote Sensing of Environment, 216, 598–614. doi:10.1016/j.rse.2018.07.014

Bolaños, R. - Hansen, L. B. - Rasmussen, M. L. - Golestani, M. - Mariegaard, J. S. - Nielsen, L. T. (2018). Coastal Bathymetry from Satellite and its use on Coastal Modelling. Coastal Engineering Proceedings, 1(36), 98. doi:10.9753/icce.v36.papers.98

Caballero, I. - Stumpf, R. P. (2000). Towards Routine Mapping of Shallow Bathymetry in Environments with Variable Turbidity: Contribution of Sentinel-2A/B Satellites Mission. Remote Sens, 12(3), 451. https://doi.org/10.3390/rs12030451

Mateo-Pérez, V. - Corral-Bobadilla, M. - Ortega-Fernández, F. - Vergara-González, E. P. (2020). Port Bathymetry Mapping Using Support Vector Machine Technique and Sentinel-2 Satellite Imagery. Remote Sensing, 12(13), 2069. https://doi.org/10.3390/rs12132069

Pacheco, A. - Horta, J. - Loureiro, C. - Ferreira, Ó. (2015). Retrieval of nearshore bathymetry from Landsat 8 images: A tool for coastal monitoring in shallow waters. Remote Sensing of Environment, 159, 102-116.

Kirwan, M. L. - Christian, R. R. - Blum, L. K. - Brinson, M. M. (2012). On the relationship between sea level and Spartina alterniflora production. Ecosystems, 15, 140-147.

Hay, A. E. - Bowen, A. J. (1993). Spatially correlated depth changes in the nearshore zone during autumn storms. Journal of Geophysical Research: Oceans, 98(C7), 12387-12404.

Gattuso, J. P. - Gentili, B. - Duarte, C. M. - Kleypas, J. A. - Middelburg, J. J. - Antoine, D. (2006). Light availability in the coastal ocean: impact on the distribution of benthic photosynthetic organisms and their contribution to primary production. Biogeosciences, 3(4), 489-513.

McFeeters, S. K. (1996). The use of the Normalized Difference water Index (NDWI) in the delineation of open water features. International Journal of Remote Sensing, 17(7), 1425-1432.

Gao, Bo-cai. (1996). NDWI – A Normalized difference water index for remote sensing of vegetation liquid water from space. Remote Sensing of Environment, 58(3), 257-266.

Xu, H. (2006). Modification of normalised difference water index (NDWI) to enhance open water features in remotely sensed imagery. International Journal of Remote Sensing, 27(14), 3025-3033.

Hedley, J. D. - Harborne, A. R. - Mumby, P. J. (2005). Simple and robust removal of sum glint for mapping shallow-water benthos. International Journal of Remote Sensing, 26(10), 2107-2112

De Keukelaere, L. - Sterckx, S. - Adriaensen, S. - Knaeps, E. - Reusen, I. - Giardino, C. - Vaiciute, D. (2018). Atmospheric correction of Landsat-8/OLI and Sentinel-2/MSI data using Icor algorithm: validation for coastal and inland waters. European Journal of Remote Sensing, 51(1), 525–542. doi:10.1080/22797254.2018.1457937

Stumpf, R. P. - Holderied, K. - Sinclair. (2003). Determination of water depth with high-resolution satellite imagery over variable bottom types. Limonol Oceanogr, 48(1, part 2), 547-556

Caballero, I. - Stumpf, R. P. (2019). Retrieval of nearshore bathymetry from Sentinel-2A and 2B satellites in South Florida coastal waters. Estuarine, Coastal and Shelf Science 226(6), 106277